View Article Online / Journal Homepage / Table of Contents for this issue
Dynamic Article Links

Journal of Materials Chemistry

Cite this: J. Mater. Chem., 2012, 22, 10200

www.rsc.org/materials

PAPER

Fuel purification, Lewis acid and aerobic oxidation catalysis performed by a microporous Co-BTT (BTT^{3-} = 1,3,5-benzenetristetrazolate) framework having coordinatively unsaturated sites†

Shyam Biswas,[a] Michael Maes,[b] Amarajothi Dhakshinamoorthy,[c] Mark Feyand,[a] Dirk E. De Vos,[b] Hermenegildo Garcia[c] and Norbert Stock*[a]

Received 1st November 2011, Accepted 23rd December 2011
DOI: 10.1039/c2jm15592c

Published on 03 February 2012 on http://pubs.rsc.org | doi:10.1039/C2JM15592C
Downloaded by Instituto de Tecnología Química on 18/04/2013 15:49:46.

Two isostructural microporous metal–organic frameworks $[Co(DMA)_6]_3[(Co_4Cl)_3(BTT)_8(H_2O)_{12}]_2 \cdot 12H_2O$ (BTT^{3-} = 1,3,5-benzenetristetrazolate; DMA = *N*,*N*′-dimethylacetamide) (**1**) and $[Cd(DMF)_6]_3[(Cd_4Cl)_3(BTT)_8(H_2O)_{12}]_2 \cdot 14H_2O \cdot 4DMF$ (DMF = *N*,*N*′-dimethylformamide) (**2**) were synthesized under solvothermal conditions. The structures of both compounds were determined by single-crystal X-ray diffraction data. Each compound adopts a porous three-dimensional framework consisting of square-planar $[M_4Cl]^{7+}$ (M^{2+} = Co, **1**; Cd, **2**) units interconnected by triangular tritopic BTT^{3-} bridging ligands to give an anionic (3,8)-connected "Moravia" net. Phase purity of the compounds was confirmed by X-ray powder diffraction (XRPD), IR spectroscopy, thermogravimetric (TG) and elemental analysis. TGA and temperature-dependent XRPD (TDXRPD) experiments indicate a moderate thermal stability up to 350 and 300 °C, respectively. Guest exchange followed by heating led to microporous solids with coordinatively unsaturated metal sites. These unsaturated metal sites create opportunities in adsorptive and catalytic applications. These have been probed by the selective removal of sulfur compounds from fuel feeds as well as the catalytic ring opening of styrene oxide and the oxidation of several cycloalkanes and benzyl compounds.

1 Introduction

Metal–organic frameworks (MOFs),[1] which are constructed from metal ions or clusters interconnected by polytopic organic linkers, have generated a great deal of interest in recent years because of their structures, diverse topologies and potential applications in areas such as gas or liquid phase adsorption and separation,[2] or catalysis.[3] The exceptionally high pore volume and surface area of MOFs allow the facile access of substrates to the catalytically active sites, either integrated at metal nodes[3,4] or located on the organic ligands.[5] The pores of MOFs can be tuned in a systematic way and hence optimized to a specific catalytic application. Besides a high density of catalytically active sites in MOFs, one of their major advantages is that all active sites are identical, because of the highly crystalline nature of the material.[4a,b] Compared to homogeneous transition metal catalysts, the heterogeneous MOF catalysts would simplify the work-up procedure by allowing simple filtration, facilitating product separation and catalyst regeneration.[6] However, some disadvantages might hamper application of MOFs in catalysis. As MOFs are synthesized under relatively mild conditions of temperature and pressure, they are mostly unstable above 600 K.[4a] Moreover, some MOFs seem to be unstable towards water in solvent concentrations, or even to atmospheric moisture.[7] The reactions catalyzed at low temperature, such as liquid phase transformations, seem to be more promising for MOFs as compared to high temperature gas phase reactions. Thus, organic synthesis and, more specifically, synthesis of fine chemicals requiring low temperature can be accomplished employing MOFs as catalysts.[1a,3b] For optimal catalytic activity, the catalytic sites must be oriented towards the pore interior and be freely accessible to substrate molecules.[4a] However, in many MOFs the metal ions are integral parts of the framework, and therefore they are completely saturated by coordination to the organic ligands.[8] Despite these drawbacks, there is an increasing number of reports showing the potentiality of MOFs in catalysis.[3,4]

In favorable cases, the removal of solvent molecules by thermal activation leads to coordinatively unsaturated metal

[a]*Institut für Anorganische Chemie, Christian-Albrechts-Universität, Max-Eyth-Strasse 2, 24118 Kiel, Germany. E-mail: stock@ac.uni-kiel.de; Fax: +49-4318801775; Tel: +49-4318801675*
[b]*Centre for Surface Chemistry and Catalysis, Katholieke Universiteit Leuven, Kasteelpark Arenberg 23, 3001 Leuven, Belgium*
[c]*Instituto Universitario de Tecnología Química CSIC-UPV and Departamento de Química, Universidad Politécnica de Valencia, Av. De los Naranjos s/n, 46022 Valencia, Spain*

† Electronic supplementary information (ESI) available: View of topological nets, XRPD patterns, TG and elemental analyses, IR, fluorescence and UV-Vis spectra, digital photos, bond lengths, reusability test for ring opening of epoxide. CCDC reference numbers 851169 and 851168. For ESI and crystallographic data in CIF or other electronic format see DOI: 10.1039/c2jm15592c

This journal is © The Royal Society of Chemistry 2012

Downloaded by Instituto de Tecnología Química on 18/04/2013 15:49:46.
Published on 03 February 2012 on http://pubs.rsc.org | doi:10.1039/C2JM15592C

sites (CUSs) which are very beneficial since CUSs can strongly interact with guest molecules such as gases and organic molecules in adsorption and catalysis. The generation of CUSs on the inner pore surface is a fundamental strategy for improving the room temperature hydrogen storage performance of MOFs.[9,10] MOFs with CUSs are also useful as potential separation materials for the capture of CO_2 from flowing gas mixtures.[11] Recently, several liquid phase separations were described like the separation of alkylaromatics and a steam cracker's C_5-cut.[12] Furthermore, the presence of CUSs was demonstrated to play a decisive role in the selective removal of *N*-heterocyclic aromatic contaminants from fuels.[13] Crude oil naturally contains sulfur compounds, which are undesirable since they cause SO_x exhaust gases. Currently, fuel feeds contain as low as 10 ppmw S and it can be expected that these levels are to be lowered further. Therefore, the complete removal of these sulfur compounds by adsorption might be an interesting application for MOFs. CUSs can be considered as Lewis acid sites. Intermediate Lewis acid sites like Co^{2+}, Cu^{2+} and Zn^{2+} have been reported to be able to interact with soft bases like typical sulfur compounds like thiophene, benzothiophene and dibenzothiophene.[14] CUS can offer a promising tool in catalysis because regular arrangements and well-defined environments of metal centers in the pore channels induce regioselectivity and shape- or size-selectivity towards guest molecules or reaction intermediates.[1b,15] In the case of Lewis acid catalyzed reactions, the availability of CUSs is a key requirement. Several MOFs having CUSs such as Cu-BTC (BTC^{3-} = benzene-1,3,5-tricarboxylate),[16] Mn-BTT (BTT^{3-} = 1,3,5-benzenetristetrazolate),[17] Fe-MIL-100 (MIL = Materials of Institute Lavoisier)[4f] and Cr-MIL-101[18] have been shown to catalyze a wide variety of organic reactions including cyanosilylation,[4a,d,19] aerobic oxidation,[20] peroxodative oxidation,[20d,21] epoxide ring opening,[22] hydrogenation,[23] acetalization,[24] *N*-methylation,[25] sulfoxidation,[26] Mukaiyama-aldol reaction,[19] Friedel–Crafts alkylation,[4f] Knoevenagel condensation,[27] Heck coupling,[27] Claisen–Schmidt condensation,[28] *etc.*[29] It is still necessary to expand the reaction types that can be catalyzed by MOFs, trying to demonstrate the advantages and limitations of these materials as catalysts, especially *versus* other common solid catalysts such as zeolites and clays.

Inspired by the above mentioned advantages, we have synthesized and fully characterized two isostructural microporous MOFs possessing CUSs, namely $[Co(DMA)_6]_3[(Co_4Cl)_3(BTT)_8(H_2O)_{12}]_2\cdot 12H_2O$ (DMA = *N*,*N*′-dimethylacetamide)(**1** or Co-BTT) and $[Cd(DMF)_6]_3[(Cd_4Cl)_3(BTT)_8(H_2O)_{12}]_2\cdot 14H_2O\cdot 4DMF$ (DMF = *N*,*N*′-dimethylformamide) (**2** or Cd-BTT). Each compound, being isotypic with the previously reported M-BTT (M^{2+} = Mn,[17] Cu,[30] or Fe[31]) materials, adopts a porous three-dimensional (3D) framework constructed of square-planar $[M_4Cl]^{7+}$ (M^{2+} = Co, **1**; Cd, **2**) units interconnected by triangular tritopic BTT^{3-} bridging ligands to give an anionic (3,8)-connected "Moravia" net. During the preparation of the manuscript, a compound having similar chemical composition and identical framework topology as **2** has been reported.[32] However, our synthetic method is different and we have been able to prove the permanent porosity of the compound. Compound **1** bears redox-active Co sites, in addition to the CUSs possessed by both compounds. Due to the partial decomposition of the framework of **2** after thermal activation, its catalytic and adsorptive features were not investigated. Compound **1**, which has a higher thermal stability, was found to catalyze the ring opening of styrene oxide, and the aerobic oxidation of several cycloalkanes and benzylic compounds. It is noteworthy that the ring opening of epoxides is an important synthetic tool for the preparation of 1,2-diols and β-alkoxyalcohols.[33] Moreover, the oxidation of C–H bonds with molecular oxygen has been a target for producing oxygenated compounds such as alcohols and ketones.[34] Furthermore, the potential of compound **1** for the selective removal of sulfur from fuel feeds has been probed by single compound adsorption isotherms.

2 Experimental

2.1 Materials and general methods

The H_3BTT ligand was synthesized according to a previously published procedure.[17] All other starting materials were of reagent grade and used as received from the commercial supplier. Fourier transform infrared (FTIR) spectra in the range 4000–400 cm^{-1} were recorded on an ATI Matheson Genesis FT-IR spectrometer from KBr pellets or an ALPHA-ST-IR Bruker spectrometer with an ATR unit. UV-Vis diffuse reflectance spectra (DRS) were recorded on a Varian Cary 5000 UV-Vis-NIR spectrophotometer in the range of 300–1100 nm and converted into normal absorption spectra with the Kubelka-Munk function.[35] Elemental analyses (C, H, N) were carried out on a Eurovector EuroEA Elemental Analyzer. Thermogravimetric analysis (TGA) was performed with a Netzsch STA-409CD thermal analyzer in a temperature range of 25–800 °C under air atmosphere at a heating rate of 4 °C min^{-1}. Ambient temperature X-ray powder diffraction (XRPD) patterns were measured using CuKα radiation (λ = 1.5406 Å) with a STOE STADI P diffractometer equipped with a linear position-sensitive detector (LPSD). Temperature-dependent X-ray powder diffraction (TDXRPD) experiments were performed under air atmosphere with a STOE STADI P diffractometer equipped with an image-plate position-sensitive detector (IPPSD) and a STOE capillary furnace (version 0.65.1) using CuKα radiation. The simulated powder patterns were calculated using data from single-crystal X-ray diffraction. The solid-state fluorescence emission spectra were collected on a Varian Cary Eclipse spectrofluorometer in the 320–550 nm region at room temperature using an excitation wavelength of 300 nm. The nitrogen, carbon dioxide and hydrogen sorption isotherms up to 1 bar were measured using a Belsorp Max apparatus at −196, 25 and −196 °C, respectively. The samples were heated at 135 °C under dynamic vacuum for 24 h prior to sorption and catalytic experiments.

Safety note! *Metal azides and tetrazolate compounds are potentially explosive, and caution should be exercised when dealing with such materials*. However, the small quantities used in this study were not found to present a hazard.

2.2 Synthesis

Elemental analyses of the compounds in different forms are presented in Table S1 (ESI†).

$[Co(DMA)_6]_3[(Co_4Cl)_3(BTT)_8(H_2O)_{12}]_2\cdot 12H_2O$ (1). A mixture of $CoCl_2\cdot 6H_2O$ (68 mg, 0.29 mmol) and H_3BTT (40 mg,

Downloaded by Instituto de Tecnología Química on 18/04/2013 15:49:46.
Published on 03 February 2012 on http://pubs.rsc.org | doi:10.1039/C2JM15592C

0.14 mmol) in 4 mL of DMA was acidified with 8 drops of HCl (2 M). The resulting solution was placed in a glass tube (10 mL). The tube was sealed and heated in a programmable oven to 130 °C at a rate of 1.8 °C min^{-1}, held at this temperature for 24 h, then cooled to room temperature at a rate of 1.8 °C min^{-1}. The supernatant was removed and the remaining red cubic crystals of **1** were washed with DMA (3 × 1 mL) and dried in air to yield 115 mg (0.01 mmol, 48%).

$[Cd(DMF)_6]_3[(Cd_4Cl)_3(BTT)_8(H_2O)_{12}]_2 \cdot 14H_2O \cdot 4DMF$ (2). A mixture of $Cd(NO_3)_2 \cdot 4H_2O$ (88 mg, 0.29 mmol) and H_3BTT (40 mg, 0.14 mmol) in 4 mL of DMF was acidified with 3 drops of HCl (2 M). The resulting solution was placed in a glass tube (10 mL). The tube was sealed and heated in a programmable oven to 70 °C at a rate of 0.8 °C min^{-1}, held at this temperature for 24 h, then cooled to room temperature at a rate of 0.8 °C min^{-1}. The resulting colorless cubic crystals of **2** were collected by filtration, washed with DMF (3 × 1 mL) and dried in air to yield 105 g (0.01 mmol, 37%).

2.3 Activation of 1 and 2

Each (0.5 g) of the as-synthesized samples of **1** and **2** was first soaked in methanol (4 × 50 mL) for 96 h, during which period, the solvent was discarded and fresh solvent was added after each 24 h. Thus, the non-coordinated and coordinated solvent molecules in **1** and **2** were exchanged with methanol molecules. In the second step, the methanol-exchanged solids were heated at 135 °C under dynamic vacuum for 24 h to remove the occluded and bound methanol molecules. After cooling to room temperature, the thermally activated compounds adsorb water from air (denoted as "hydrated form" hereafter).

2.4 Single-crystal X-ray diffraction

Structures of **1** and **2** were determined from single-crystal X-ray diffraction data. Single-crystal X-ray diffraction intensities of **1** and **2** were collected on a STOE IPDS diffractometer employing monochromated MoKα radiation (λ = 0.71073 Å) at 293 and 200 K, respectively. Initial structures were solved by direct methods and refined by full-matrix least-squares techniques based on F^2 using the SHELXL-97 program.[36] Details of single-crystal data collection and refinement of **1** and **2** are summarized in Table 1.

2.5 Catalytic experiments

Preparation of the *N*-hydroxyphthalimide (NHPI)/1 catalyst. NHPI (200 mg) (1 wt%) was dissolved in 7 mL of dichloromethane and 3 mL of methanol. To this solution, 1 g of solid **1** (corresponding to a 5 wt% of NHPI) was added and the resulting suspension was heated at 40 °C for 4 h. After the required time, the mixture was cooled and the solvent was removed by rotary evaporation. The resulting solid was dried at 80 °C for 2 h.

Typical experimental procedure. Styrene oxide (0.1 mL) in methanol (5 mL), cyclooctane (2 mL) or the benzylic compounds (2 mL) and the corresponding catalyst (20 or 50 mg for methanolysis or aerobic oxidation, respectively) were placed in a two-necked flask (10 mL). For aerobic oxidation, the flask was equipped with a balloon filled with molecular oxygen. The mixture was stirred at 50 °C (methanolysis of styrene oxide), 100 °C (toluene oxidation) or 120 °C (cyclooctane and rest of benzylic oxidations) for the required time as mentioned in Table 3. Blank reactions at these temperatures showed no catalytic conversions of the substrates. The course of the oxidation was followed by analyzing four aliquots (2 μL) of the reaction mixture collected with a microsyringe. At the end of the reaction, the heterogeneous mixture was cooled, diluted with acetonitrile and methanol, and filtered. The liquid phase was dried over anhydrous $MgSO_4$. The conversion, purity and yield of the final products were determined using a Hewlett Packard 5890 series II gas chromatograph with a FID detector and high purity helium as carrier gas. The products were identified by comparing their retention times in GC with authentic samples and with GC-MS Hewlett Packard 6890 series. Quantification was performed using *n*-dodecane as GC external standard. To a known aliquot of the sample, a given amount of *n*-dodecane was added and the solution was injected in the GC to determine the degree of conversion and selectivity. The corresponding response factors of the substrates and products were used to transform relative peak areas into molar ratios. Under the present experimental conditions, oxidation of the external standard was not observed. The identity of the products was confirmed by GC-MS and also by co-injection of authentic samples. Personal safety items have to be used to minimize the risks when using mixtures of alkanes and oxygen. For most of the alkanes studied in the present work, the boiling point is higher than the working temperature. All the reactions were performed in a sealed glass reactor fitted with a condenser. The reactions were carried out under an oxygen saturated atmosphere.

Detection of octanedioic acid. Aerobic oxidation reaction of cyclooctane was carried out as described in the previous section. After 24 h, the reaction mixture was diluted with acetonitrile and methanol, and the catalyst was filtered off. The filtrate was subjected under reduced pressure to remove all the volatile compounds. To the resulting residue (pale yellow oil), 1 mL *N*, *O*-bis(trimethylsilyl)trifluoroacetamide with trimethylchlorosilane was added and the resulting solution was heated at 80 °C for 6 h. The reaction mixture was diluted with acetonitrile and injected in GC-MS. The formation of the disilylated product of dicarboxylic acid (7%) was observed.

To confirm that most of the octanedioic acid can be quantified using this procedure, a known quantity of adipic acid (100 mg, 5 wt%) was added to the cyclooctane (2 mL) suspension of the NHPI/**1** catalyst and the suspension was heated at 120 °C for 6 h under inert atmosphere. After this time, the reaction mixture was diluted with acetonitrile and methanol and filtered off. After removing the solvent and cyclooctane under reduced pressure, 95% of the initial amount of adipic acid was quantified.

Experimental procedure for reusability. The reusability of NHPI/**1** was tested for oxidation of cyclooctane. At the end of the reaction, the reaction mixture was diluted with acetonitrile and methanol, and filtered off. The filtered catalyst was dried at 60 °C for 2 h and reused directly without further purification for the second run.

 This journal is © The Royal Society of Chemistry 2012

Table 1 Single-crystal X-ray data and structure refinement parameters for **1** and **2**. The reported compositions of the compounds are based on the crystal structure refinement. The final structural model was refined without the guest molecules in the pores by using the SQUEEZE option implemented in the program PLATON[43]

Compound	**1**	**2**
Formula	$C_{24}H_8ClCo_4N_{32}O_4$	$C_{24}H_8Cd_4ClN_{32}O_4$
Formula mass	1079.79	1293.71
T/K	293(2)	200(2)
λ/Å	0.71073	0.71073
Crystal dimensions/mm	0.10 × 0.10 × 0.10	0.07 × 0.07 × 0.07
Crystal system	Cubic	Cubic
Space group	$Pm\bar{3}m$	$Pm\bar{3}m$
a/Å	18.739(2)	19.357(2)
V/Å^3	6580.0(13)	7252.5(14)
Z	3	3
D_c/g cm^{-3}	0.817	0.889
μ/mm^{-1}	0.810	0.928
F(000)	1599	1851
θ Range/°	1.54–28.03	2.10–26.00
Measured reflections	65 999	31 576
Independent reflections/R_{int}	1619/0.0579	1474/0.1063
Data/restraints/parameters	1619/0/47	1474/0/47
R_1 ($I > 2\sigma(I)$)[a]	0.0782	0.0406
wR_2 (all data)[b]	0.2379	0.1058
Goodness-of-fit on F^2	1.251	1.142
$\Delta\rho_{max,min}$/eÅ^{-3}	1.106, −1.090	1.072, −0.924

[a] $R_1 = \sum||F_o| - |F_c||/\sum|F_o|$. [b] $wR_2 = \{\sum[w(F_o^2 - F_c^2)^2]/\sum[w(F_o^2)^2]\}^{1/2}$.

2.6 Adsorption experiments

Liquid phase batch adsorption experiments were carried out in 1.8 mL glass vials filled with 0.025 g of activated compound **1** and a solution of heptane : toluene in a volumetric ratio of 80 : 20 contaminated with sulfur compounds at 25 °C following a literature procedure.[12a,37] Uptakes were directly calculated from GC output data.

3 Results and discussion

3.1 Synthesis

In order to check the generality of formation of the M-BTT framework structures, reactions analogous to those employed in forming Cu-BTT and Mn-BTT were attempted using either chloride salts, or a combination of dilute hydrochloric acid and nitrate salts of a series of first-row transition-metal ions (Fe^{2+}–Zn^{2+}) and Cd^{2+} ion. The amide solvents used included DMF, *N*,*N*′-diethylformamide (DEF), DMA, *N*-methyl-2-pyrrolidone (NMP) and the reaction temperatures used ranged from 60 °C to 140 °C. In addition to previously reported M-BTT (M^{2+} = Mn, Cu, and Fe) materials,[17,30,31] highly crystalline solids have been achieved with Co^{2+} and Cd^{2+} salts. It is worthy to mention that the guest Mn^{2+} ions in the methanol-exchanged form of Mn-BTT $Mn_3[(Mn_4Cl)_3(BTT)_8(CH_3OH)_{10}]_2$ have been formerly exchanged with cations such as Li^+, Cu^+, Fe^{2+}, Co^{2+}, Ni^{2+}, Cu^{2+} and Zn^{2+} to produce a wide variety of isostructural bimetallic framework solids.[38]

3.2 Structure description

The single-crystal X-ray diffraction studies reveal that the framework topologies of both **1** and **2** are identical, and they correspond to the M-BTT (M^{2+} = Mn, Cu or Fe)[17,30,31] structure previously reported by the Long group. As displayed in Fig. 1, the cubic (space group: $Pm\bar{3}m$) structures are built of chloride-centered square-planar $[M_4Cl]^{7+}$ (M^{2+} = Co, **1**; Cd, **2**) units which are interconnected with triangular planar BTT^{3-} ligands to form an anionic, 3D framework. The M^{2+} ions of the $[M_4Cl]^{7+}$ squares are bridged by tetrazolate rings from eight BTT ligands *via* their N^2 and N^3 donor atoms. Similarly, each BTT ligand is connected with three $[M_4Cl]^{7+}$ units. Thus, six $[M_4Cl]^{7+}$ units and eight BTT ligands, each of which is coordinated with six adjacent M^{2+} ions, describe the square and hexagonal faces of a truncated octahedron, respectively. The truncated octahedron resembles a sodalite cage. Each sodalite-like cage is connected with six adjacent cages through its square faces, thus constructing a network closely related to that of sodalite. However, the topological connectivity of the network is completely different from that of sodalite. The trigonal planar BTT linkers and the square-planar $[M_4Cl]^{7+}$ units surrounded by eight tetrazolates can be considered as 3- and 8-connected nodes, respectively, to construct a 3D (3,8)-connected framework (Fig. S1†). In TOPOS[39] and RCSR[40] databases, this unique topological connectivity has been named as the "Moravia" net, which was recently predicted to exist.[41] Five metal–tetrazolate (M = Mn, Fe, Cu)[17,30,31] frameworks isostructural to **1** and **2**, along with three metal–carboxylate (M = Fe, Co, Cu)[42] networks, have yet been reported to adopt this topological net. Notably, the report of the carboxylate-based framework $H_6[(Co_4O)_3(TATB)_8]$ (H_3TATB = 4,4′,4″-s-triazine-2,4,6-triyltribenzoic acid)[42a] having the same "Moravia" topology affirms the similarities between tetrazolate- and carboxylate-based bridging linkers. Both frameworks are anionic having formula $[(M_4Cl)_3(BTT)_8(H_2O)_{12}]^{3-}$. The sixth coordination site of each octahedrally coordinated M^{2+} ion is provided by water molecules. For both compounds, $[M(solvent)_6]^{2+}$ ions situated inside the sodalite-like cages balance the charge so that the overall compounds appear as electrostatically neutral.

Published on 03 February 2012 on http://pubs.rsc.org | doi:10.1039/C2JM15592C
Downloaded by Instituto de Tecnología Química on 18/04/2013 15:49:46.

Downloaded by Instituto de Tecnología Química on 18/04/2013 15:49:46.
Published on 03 February 2012 on http://pubs.rsc.org | doi:10.1039/C2JM15592C

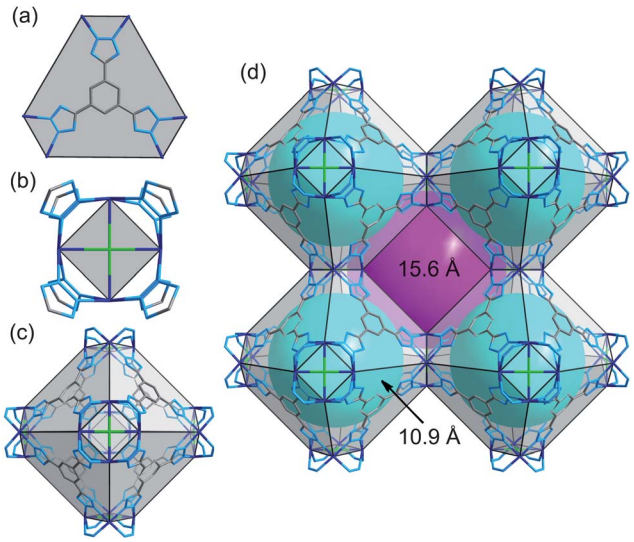

Fig. 1 Views of the frameworks of **1** and **2** in wire representation (color codes: N, light blue; Co or Cd, dark blue; C, grey, Cl, green). (a) BTT ligand connected with six neighbouring M^{2+} ions constructing the 3-connected node and hexagonal face. (b) Four M^{2+} ions bridged by eight tetrazolate rings forming the 8-connected node and square face. (c) A sodalite-like cage constructed from six $[M_4Cl]^{7+}$ units and eight BTT linkers located at its square and hexagonal faces, respectively. (d) A cube of eight cages, each of which is connected with six adjacent cages through its square faces. The void cavity inside the cages and the one formed by connecting eight such cages are displayed as cyan and magenta spheres, respectively. For clarity, hydrogen atoms and coordinated water molecules have been removed from all structural plots.

Taking the van der Waals radii of C atoms (1.75 Å) into account, imaginary spheres with diameters of 10.9 and 15.6 Å could fit into the sodalite-like cages and the larger cages formed by eight sodalite-like cages, respectively. The nearly circular cage window between the larger cages would admit the passage of an imaginary sphere with a diameter of 10.2 Å, taking the van der Waals radii of N atoms (1.55 Å) into account. The M–N distances of **1** and **2** are 2.098(3) and 2.329(3) Å, respectively. The M–O distances observed in **1** and **2** are 2.082(7) and 2.301(8) Å, respectively. The solvent accessible volumes of **1** and **2** estimated by the program PLATON[43] are 4384.2 and 4934.9 $Å^3$, respectively, which are 66.6% and 68.0% of the respective unit cell volumes (6580.0 $Å^3$, **1**; 7252.5 $Å^3$, **2**). The counter ions or solvent molecules inside the pores could not be refined owing to the severe thermal disorder, and they were characterized by the IR spectroscopy, TGA and elemental analysis. The final structural model was refined without the counter ions or solvent molecules by using the SQUEEZE option implemented in the program PLATON.[43]

4 TGA and XRPD

Phase purity of **1** and **2** was examined using XRPD patterns recorded from as-synthesized **1** and **2** at ambient conditions. The experimental XRPD patterns of **1** and **2** (Fig. S2 and S3†) are consistent with the simulated ones as gleaned from the single-crystal X-ray diffraction data. The compounds retain their crystallinity upon soaking in methanol and consequent heating at 135 °C for 24 h under dynamic vacuum (*i.e.*, activation), as verified by the XRPD patterns of the corresponding samples (Fig. S4 and S5†). Moreover, TGA and temperature-dependent XRPD (TDXRPD) experiments were performed to examine the thermal stability of both compounds. It is observed that as-synthesized **1** and **2** decompose above 350 and 300 °C, respectively.

In the TG curve of as-synthesized **1** (Fig. 2a), the first weight loss of 8.3% in the range 25–120 °C is attributed to the removal of 12 guest water molecules per formula unit (calc. 7.6%). The second weight loss of 16.5% in the range of 120–270 °C is due to the removal of 18 DMA molecules per formula unit (calc. 18.5%). After that the framework starts to decompose leading to the formation of an X-ray amorphous material. Below the decomposition temperature, the first weight loss steps of 29.5 and 22.9% are assigned to the removal of 82 methanol and 104 water molecules for methanol-exchanged and hydrated **1** (Fig. S8 and S9†), respectively (calc. 29.5 and 23.0%).

TDXRPD analysis (Fig. 2b) shows that as-synthesized **1** is stable up to 350 °C. After that the compound starts to decompose and becomes completely amorphous at 400 °C.

In the TG curve of as-synthesized **2** (Fig. 3a), the first weight loss of 7.8% in the range 25–120 °C is assigned to the loss of 14 non-coordinated water molecules per formula unit (calc. 6.8%). The second weight loss of 16.2% in the range of 120–270 °C is due to the removal of 22 molecules of occluded DMF molecules per formula unit (calc. 16.0%). After that decomposition of the compound occurs resulting in the formation of CdO. Below the decomposition temperature, the first weight loss steps of 25.4 and 18.6% are assigned to the removal of 82 methanol and 98 water molecules for methanol-exchanged and hydrated **2** (Fig. S10 and S11†), respectively (calc. 25.4 and 18.6%).

From the TDXRPD patterns (Fig. 3b), it becomes obvious that as-synthesized **2** is stable up to 300 °C. After that the material starts to decompose and becomes completely amorphous at 300 °C.

5 FT-IR, luminescence and UV-Vis spectroscopy

The FT-IR spectra of the as-synthesized, methanol-exchanged and thermally activated samples of isostructural **1** and **2** (Fig. S6 and S7†) are almost identical, as expected. The characteristic

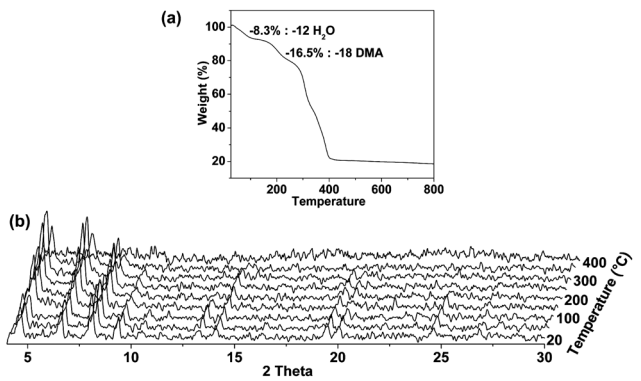

Fig. 2 (a) TG analysis of as-synthesized **1** under air atmosphere. (b) TDXRPD plots of as-synthesized **1** in the range of 20–400 °C.

 This journal is © The Royal Society of Chemistry 2012

Downloaded by Instituto de Tecnología Química on 18/04/2013 15:49:46.
Published on 03 February 2012 on http://pubs.rsc.org | doi:10.1039/C2JM15592C

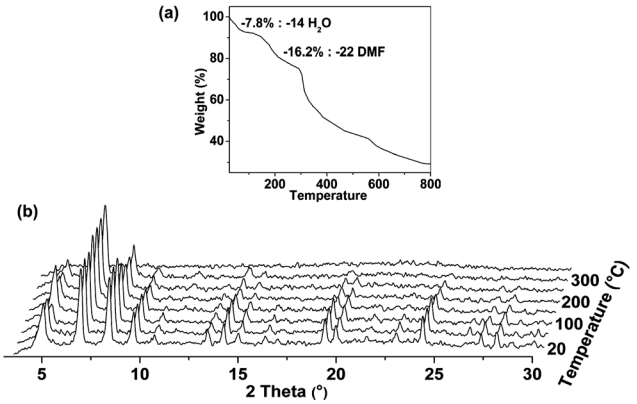

Fig. 3 (a) TG analysis of as-synthesized **2** under air atmosphere. (b) TDXRPD plots of as-synthesized **2** in the range of 20–350 °C.

strong absorption bands assignable to carbonyl groups of occluded DMA and DMF molecules appear at 1613 and 1658 cm^{-1} in the IR spectra of as-synthesized **1** and **2**, respectively.[44] In the IR spectra of methanol-exchanged **1** and **2**, the carbonyl stretching bands of amide solvent molecules are absent, and a new absorption band attributable to the C–O stretching frequency of the methanol molecule is present at 1019 cm^{-1}.[17,30,31] These changes indicate that the amide solvent molecules are completely exchanged by the methanol molecules. The absence of the strong bands at 1019 cm^{-1} in the IR spectra of thermally activated **1** and **2** suggests that methanol molecules have been removed from methanol-exchanged **1** and **2**.

Inspired by the strong fluorescence emissions of previously reported coordination polymers containing tetrazolate ligands and d^{10} metal ions,[45] we investigated the luminescent properties of the as-synthesized sample of Cd-based **2**. Upon excitation at a wavelength of 300 nm, free H_3BTT ligand exhibits a sharp, strong emission band at 350 nm and a weak, broad band centered at 415 nm (Fig. S12†). Because the sharp emission band of as-synthesized **2** occurs at the similar position (340 nm) to that of the free H_3BTT ligand, it should be assigned to the intraligand π–π^* transition of the BTT ligand.

The solid-state UV-Vis spectra of as-synthesized **1** (Fig. S13†) display three absorption peaks at 1030, 500 and 450 nm in the visible region, which can be attributed to the spin-allowed transitions $^4T_{1g}(F) \rightarrow {}^4T_{2g}(F)$ (ν_1), $^4T_{1g}(P)$ (ν_2), and $^4A_{2g}$ (ν_3), respectively.[46] The calculated values of Dq (1110 cm^{-1}) and B (925 cm^{-1}) from these transitions are comparable to those of other compounds with octahedrally coordinated Co^{2+} ions.[46] The absorption band at 450 nm is very weak for thermally activated **1** due to the change of the coordination environment of Co^{2+} ions from octahedral to square-pyramidal as a result of removal of coordinated methanol molecules. The coordination transition of Co^{2+} ions is also verified by the change of color of as-synthesized **1** from red to grayish pink after thermal activation (Fig. S14†).

6 Gas sorption properties

N_2, CO_2 and H_2 sorption studies were performed on thermally activated **1** and **2**. The results of the sorption analysis are presented in Table 2. The sorption capacities of the present compounds are comparable with the previously reported Mn-BTT,[17] Cu-BTT[30] and Fe-BTT[31] compounds.

The N_2 adsorption and desorption measurements carried out with thermally activated **1** and **2** revealed reversible type-I isotherms (Fig. 4) with a small hysteresis loop in the p/p_0 region of 0.5–1.0 at −196 °C.

The CO_2 adsorption properties of thermally activated **1** and **2** were investigated at 25 °C up to 1 bar. As shown in Fig. 5, the CO_2 adsorption isotherms of both compounds follow type-I behavior in the pressure range from 0 to 1 bar. The lower CO_2 uptake of **2** (Table 2) can be attributed to the partial decomposition of the framework after thermal activation leading to the significant loss of crystallinity of the material, as verified by X-ray powder diffractometry (Fig. S5†).

The hydrogen adsorption isotherms of thermally activated **1** and **2** follow reversible type-I behavior (Fig. 6) at −196 °C up to 1 bar.

7 Selective removal of sulfur compounds from fuel feeds

The smaller sodalite-like cages of compound **1** are likely inaccessible to larger organic molecules since the cage windows between the smaller and the larger cages are too small. However, the cage windows between the larger cages have a diameter of 10.2 Å and are thus sufficiently large to allow larger organic molecules, as typically encountered in the liquid phase, to diffuse through. Since these large cages contain CUSs, the potential of compound **1** for the selective removal of sulfur compounds from fuel feeds has been probed by measuring the single compound adsorption isotherms of thiophene, benzothiophene and dibenzothiophene out of a synthetic mixture of heptane : toluene in a volumetric ratio 80 : 20 (H/T 80/20), a mixture that simulates an actual fuel feed composition (Fig. 7).

Single compound isotherms reveal the selective uptake of all three sulfur compounds tested. Thiophene is adsorbed up to 2 wt%, while benzothiophene and dibenzothiophene reach saturation levels of 7 and 11 wt%, respectively. These results correspond to an uptake of 2.5 molecules of thiophene per unit cell, 4 molecules of benzothiophene and even 4.5 molecules of dibenzothiophene per unit cell. A unit cell comprises half a large supercage and 1 complete sodalite-type cage and it contains 8 CUSs per half a large supercage.

It has been reported that toluene, abundantly present as solvent molecules, co-adsorbs in MOFs with CUSs on the less specific adsorption sites like the aromatic rings in the pore walls.[13] Therefore, adsorption of these sulfur compounds can be assumed to occur mainly on the CUSs. Co^{2+} can be considered as an intermediate Lewis acid site and will be able to interact with weak bases like sulfur compounds and toluene molecules. The uptake of thiophene is relatively low, with approximately one out of three CUS occupied. Thiophene is smaller than (di)benzothiophene and will thus only be able to interact with the CUSs. Since the aromatic ring of toluene molecules will also be able to interact with these CUSs, not all of these sites will be occupied by thiophene, resulting in a fairly low uptake.

In the case of benzothiophene and dibenzothiophene, up to 4.5 molecules can be adsorbed in the unit cell of compound **1**. In addition to their sulfur atoms, these compounds can interact by

Table 2 Results of sorption analysis for the M-BTT (M^{2+} = Co, Cd, Mn, Cu, Fe) solids

Compound	BET surface area[a]/m^2 g^{-1}	Langmuir surface area[a]/m^2 g^{-1}	Micropore volume[a] at $p/p_0 = 0.5$ (cm^3 g^{-1})	H_2 uptake at 1 bar (wt%)	CO_2 uptake at 1 bar (wt%)
Co-BTT	1749	1993	0.67	1.5	13.7
Cd-BTT	1415	1635	0.58	1.4	6.2
Mn-BTT[17]	2100	—	—	2.3	—
Cu-BTT[30]	1710	1770	—	2.4	—
Fe-BTT[31]	2010	2200	—	2.3	13.5

[a] The specific surface areas and micropore volumes have been calculated from the N_2 adsorption isotherms.

Downloaded by Instituto de Tecnología Química on 18/04/2013 15:49:46.
Published on 03 February 2012 on http://pubs.rsc.org | doi:10.1039/C2JM15592C

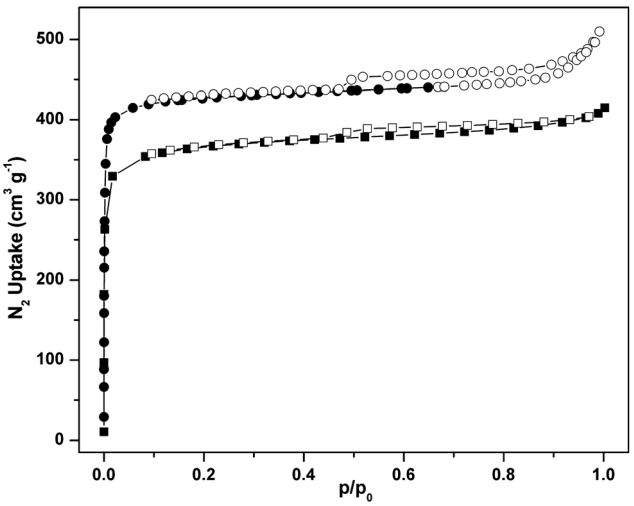

Fig. 4 Low pressure N_2 adsorption (solid symbols) and desorption (empty symbols) isotherms of thermally activated **1** (circles) and **2** (squares) measured at −196 °C.

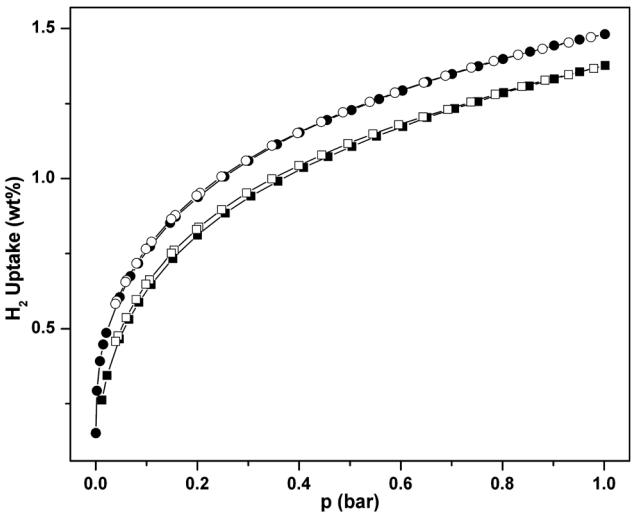

Fig. 6 Low pressure H_2 adsorption (solid symbols) and desorption (empty symbols) isotherms of thermally activated **1** (circles) and **2** (squares) measured at −196 °C.

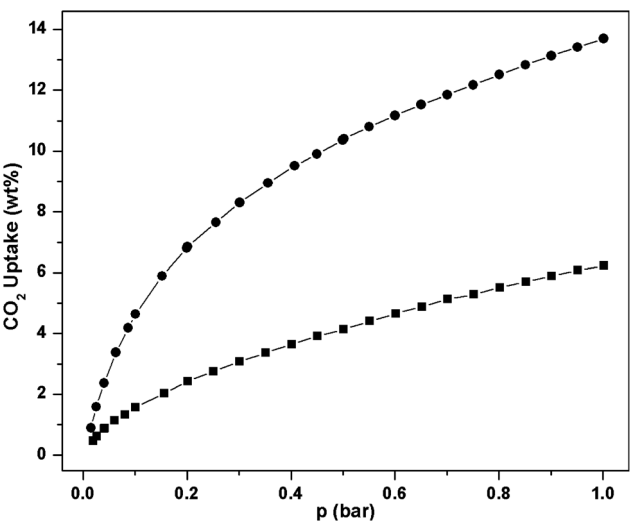

Fig. 5 CO_2 adsorption isotherms of thermally activated **1** (circles) and **2** (squares) measured at 25 °C.

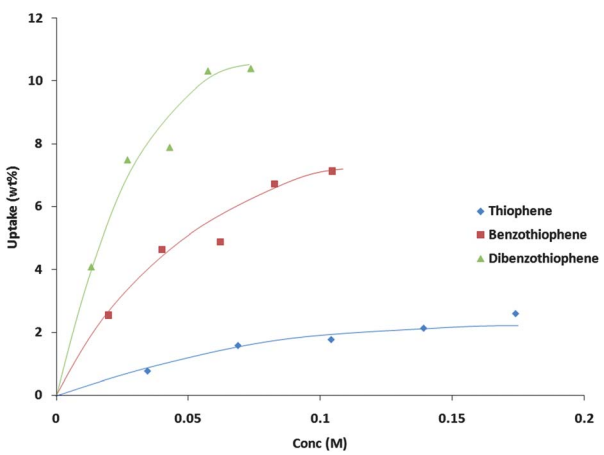

Fig. 7 Single compound adsorption isotherms measured in the batch mode: uptake (wt%) of thiophene, benzothiophene or dibenzothiophene out of a mixture of H/T 80/20 as a function of equilibrium concentration (*M*). Experiments were performed at room temperature (25 °C).

means of their own aromatic rings with, for example, the organic linker in the pore walls. π–π interactions between the aromatic rings of adsorbate molecules and organic linkers of the host have been extensively reported.[47] This additional interaction leads to a more pronounced uptake of these aromatic ring containing sulfur compounds compared to thiophene. The fact that not all free ligation sites are occupied can be explained by the cage dimensions. It is logic to assume that these larger molecules can only be adsorbed in limited amounts before the cages are completely saturated. In addition to this, the adsorption of

 This journal is © The Royal Society of Chemistry 2012

Downloaded by Instituto de Tecnología Química on 18/04/2013 15:49:46.
Published on 03 February 2012 on http://pubs.rsc.org | doi:10.1039/C2JM15592C

(di)benzothiophene on one free metal site might sterically hinder the adsorption on a nearby free metal site. In this case, these metal sites will likely be occupied by smaller toluene solvent molecules.

8 Catalytic properties

Encouraged by the availability of both Lewis acidic and potentially redox-active Co sites in thermally activated **1**, we have investigated its catalytic performance in the ring opening of styrene epoxide and in the aerobic oxidation of different cycloalkanes and benzylic compounds.

8.1 Ring opening of styrene oxide

The previously reported Mn-BTT compound, which is isostructural to **1**, was shown to exhibit size-selective Lewis acid catalysis in the cyanosilylation of carbonyl substrates and in the Mukaiyama-aldol reaction.[19] Selecting ring opening of epoxide as the model reaction, we have screened the methanolysis of styrene oxide in the presence of thermally activated **1**. The time-conversion plot for the transformation of styrene oxide with methanol as a nucleophile to 2-methoxy-2-phenylethanol is shown in Fig. 8. The conversions of the substrate to the product were 67 and 40% after 29 h in the presence of thermally activated **1** and $Co(NO_3)_2 \cdot 6H_2O$ (Fig. 8a and c), respectively. This fact confirms the higher efficiency of thermally activated **1** compared to the homogeneous catalyst.

To verify whether the catalysis of ring opening of styrene oxide with methanol is truly heterogeneous or is due to some leached Co^{2+} ions present in the liquid phase, the reaction was carried out under the optimized conditions at 50 °C using thermally activated **1** as catalyst. Then, the solid was filtered in hot from the reaction mixture after 9 h at 30% formation of 2-methoxy-2-phenylethanol. After removal of catalyst **1**, the solution in the absence of solid was again stirred at 50 °C. After 29 h, no further product formation was observed in the absence of solid (Fig. 8b).

Reusability of **1** as a heterogeneous catalyst for the ring opening of styrene oxide was investigated under optimized conditions at 50 °C. After the reaction time, the solid catalyst was filtered, washed with methanol, heated at 135 °C for 24 h under vacuum, and used for another consecutive run without further treatment. The catalyst exhibited very minor decrease in percentage conversions upon reuse for the second and third runs (Fig. S15†). A comparison of the XRD patterns of the fresh and thrice-used sample of **1** (Fig. S4†) verifies the structural integrity of thermally activated **1** under the catalytic conditions.

8.2 Aerobic oxidation of cycloalkanes and benzylic compounds

Besides as solid Lewis acid, we also studied the activity of solid **1** to promote the aerobic oxidation of C–H bonds in combination with *N*-hydroxyphthalimide (NHPI) as radical initiator. It is well documented in the literature that NHPI in combination with Co^{2+} salts is a powerful homogeneous catalyst for the aerobic oxidation of alkanes, alcohols and other organic compounds.[48] We have recently shown that NHPI adsorbed within the pores of commercial Fe(BTC) is an efficient catalyst for the selective oxidation of cycloalkanes.[49] It can be assumed that other MOFs,

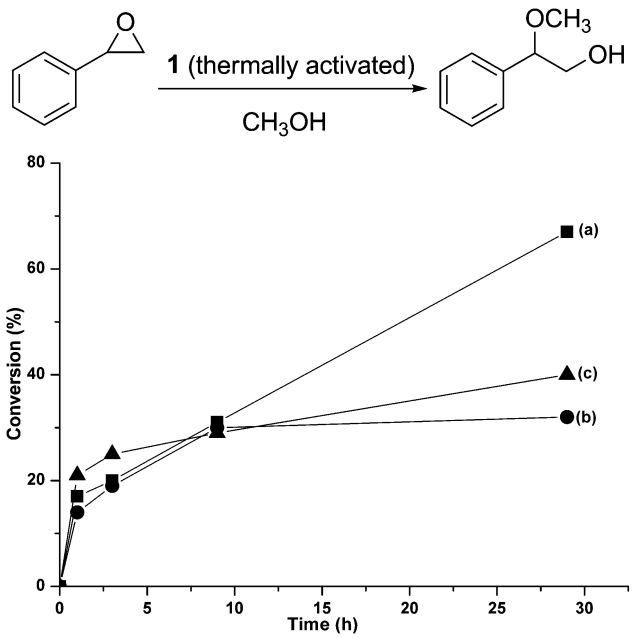

Fig. 8 Time conversion plot for the ring opening of styrene oxide in methanol with: (a) thermally activated **1**, (b) removal of the catalyst, and (c) $Co(NO_3)_2 \cdot 6H_2O$. *Reaction conditions*: (a) styrene oxide (0.1 mL), thermally activated **1** (20 mg), methanol (5 mL), 50 °C; (b) same as conditions given in "a" with removal of the catalyst after 9 h; (c) styrene oxide (0.1 mL), $Co(NO_3)_2 \cdot 6H_2O$ (34 mg), methanol (5 mL), 50 °C. The scheme for the reaction is shown on the top.

Table 3 Aerobic oxidation of cycloalkanes and benzylic compounds using NHPI/**1**[a]

Run	Substrate	Time/h	Conversion (%)[b]	Selectivity (%)[b] ol/one	Others
1		1	—		
2		4	3	99[c]	
3		9	7	99[c]	
4		24	—	—	—
5	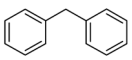	1	5	99[c]	—
6		4	10	99[c]	—
7		9	14	99[c]	—
8		29	20	99[c]	—
9		1	3	98	—
10		4	13	98	—
11		9	34	95	5[d]
12		29	41	93	7[d]
13		1	1.3	98	2
14		4	13	97	3
15		9	25	96	4
16		29	48	78	22[e]

[a] *Reaction conditions*: substrate (2 mL), NHPI/**1** (50 mg, having 5 wt% loading of NHPI), 120 °C, oxygen purged; in the case of toluene at 100 °C. [b] Determined by GC. [c] Selectivity corresponds to ketone. [d] Small percentage of tetralin hydroperoxide, 1-naphthol and 1,4-benzoquinone was also formed. [e] This number corresponds to the combined selectivity of cyclooctylhydroperoxide, cyclooctanediol, cyclooctanedione, octanedioic acid.

Downloaded by Instituto de Tecnología Química on 18/04/2013 15:49:46.
Published on 03 February 2012 on http://pubs.rsc.org | doi:10.1039/C2JM15592C

particularly those containing Co^{2+}, having NHPI incorporated inside the pores, can also act similarly.

The aerobic oxidation of several cycloalkanes and benzylic compounds in the presence of solid **1** containing NHPI was examined. The results of the catalytic activity are presented in Table 3.

Comparison of the results achieved using NHPI/**1** with those recently reported for the analogous NHPI/Fe(BTC) system indicates that **1** as host exhibits lower activity, but a higher selectivity towards ol/one at the same conversion level. Considering that selectivity is the key issue in aerobic oxidations, it seems that solid **1** containing Co^{2+} should be a preferable catalyst than Fe(BTC).

9 Conclusions

Summarizing, we have discovered two new micoporous MOFs: Co-BTT (**1**) and Cd-BTT (**2**) using 1,3,5-benzenetristetrazole (H_3BTT) as linker and a solvothermal approach in two different amide solvents (DMA for **1**; DMF for **2**). The successful synthesis and characterization of these two compounds generalize the feasibility of synthesizing microporous M-BTT frameworks with most of the 3d (Mn, Fe, Co, Cu) along with a 4d (Cd) transition metal(II) ion. Both compounds are highly porous and promising for gas phase adsorption and storage applications. The availability of CUSs reveals the compounds potential for the purification of fuel feeds and these CUSs as well as redox-active Co sites enabled the thermally activated Co-BTT solid as a heterogeneous catalyst in the ring opening of styrene oxide, and in the aerobic oxidation of several cycloalkanes and benzylic compounds.

Acknowledgements

The Deutsche Forschungsgemeinschaft (DFG, SPP 1362 "Porous Metal–Organic Frameworks" under the grant STO 643/5-2) is gratefully acknowledged for the financial support. The research leading to these results has received funding from the European Community's Seventh Framework Programme (FP7/2007-2013) under grant agreement no. 228862.

References

1 (*a*) G. Férey, *Chem. Soc. Rev.*, 2008, **37**, 191; (*b*) S. Kitagawa, R. Kitaura and S. Noro, *Angew. Chem., Int. Ed.*, 2004, **43**, 2334; (*c*) O. M. Yaghi, M. O'Keeffe, N. W. Ockwig, H. K. Chae, M. Eddaoudi and J. Kim, *Nature*, 2003, **423**, 705.

2 (*a*) L. J. Murray, M. Dincă and J. R. Long, *Chem. Soc. Rev.*, 2009, **38**, 1294; (*b*) J.-R. Li, R. J. Kuppler and H.-C. Zhou, *Chem. Soc. Rev.*, 2009, **38**, 1477; (*c*) L. Hamon, P. L. Llewellyn, T. Devic, A. Ghoufi, G. Clet, V. Guillerm, G. D. Pirngruber, G. Maurin, C. Serre, G. Driver, W. van Beek, E. Jolimaitre, A. Vimont, M. Daturi and G. Férey, *J. Am. Chem. Soc.*, 2009, **131**, 17490.

3 (*a*) A. Corma, H. Garcia and F. X. Llabres i Xamena, *Chem. Rev.*, 2010, **110**, 4606; (*b*) D. Farrusseng, S. Aguado and C. Pinel, *Angew. Chem., Int. Ed.*, 2009, **48**, 7502; (*c*) J. Y. Lee, O. K. Farha, J. Roberts, K. A. Scheidt, S. T. Nguyen and J. T. Hupp, *Chem. Soc. Rev.*, 2009, **38**, 1450; (*d*) Z. Wang, G. Chen and K. Ding, *Chem. Rev.*, 2009, **109**, 322; (*e*) L. Ma, C. Abney and W. Lin, *Chem. Soc. Rev.*, 2009, **38**, 1248.

4 (*a*) K. Schlichte, T. Kratzke and S. Kaskel, *Microporous Mesoporous Mater.*, 2004, **73**, 81; (*b*) C. Janiak, *Dalton Trans.*, 2003, 2781; (*c*) L. Alaerts, E. Seguin, H. Poelman, F. Thibault-Starzyk, P. A. Jacobs and D. E. De Vos, *Chem.–Eur. J.*, 2006, **12**, 7353; (*d*) A. Henschel, K. Gedrich, R. Kraehnert and S. Kaskel, *Chem. Commun.*, 2008, 4192; (*e*) J. W. Han and C. L. Hill, *J. Am. Chem. Soc.*, 2007, **129**, 15094; (*f*) P. Horcajada, S. Surblé, C. Serre, D. Y. Hong, Y. K. Seo, J. S. Chang, J. M. Greneche, I. Margiolaki and G. Férey, *Chem. Commun.*, 2007, 2820.

5 (*a*) S. Hasegawa, S. Horike, R. Matsuda, S. Furukawa, K. Mochizuki, Y. Kinoshita and S. Kitagawa, *J. Am. Chem. Soc.*, 2007, **129**, 2607; (*b*) C. Wu, A. Hu, L. Zhang and W. Lin, *J. Am. Chem. Soc.*, 2005, **127**, 8940; (*c*) Y. K. Hwang, D.-Y. Hong, J.-S. Chang, S. H. Jhung, Y.-K. Seo, J. Kim, A. Vimont, M. Daturi, C. Serre and G. Férey, *Angew. Chem., Int. Ed.*, 2008, **47**, 4144; (*d*) M. J. Ingleson, J. P. Barrio, J. Bacsa, C. Dickinson, H. Park and M. J. Rosseinsky, *Chem. Commun.*, 2008, 1287; (*e*) K. S. Suslick, P. Bhyrappa, J. H. Chou, M. E. Kosal, S. Nakagaki, D. W. Smithenry and S. R. Wilson, *Acc. Chem. Res.*, 2005, **38**, 283; (*f*) S. H. Cho, B. Ma, S. T. Nguyen, J. T. Hupp and T. E. Albrecht-Schmitt, *Chem. Commun.*, 2006, 2563; (*g*) A. M. Shultz, O. K. Farha, J. T. Hupp and S. T. Nguyen, *J. Am. Chem. Soc.*, 2009, **131**, 4204; (*h*) J. S. Seo, D. Whang, H. Lee, S. I. Jun, J. Oh, Y. J. Jeon and K. Kim, *Nature*, 2000, **404**, 982; (*i*) O. R. Evans, H. L. Ngo and W. Lin, *J. Am. Chem. Soc.*, 2001, **123**, 10395; (*j*) A. G. Hu, H. L. Ngo and W. Lin, *J. Am. Chem. Soc.*, 2003, **125**, 11490; (*k*) A. Hu, H. L. Ngo and W. Lin, *Angew. Chem., Int. Ed.*, 2003, **42**, 6000; (*l*) D. N. Dybtsev, A. L. Nuzhdin, H. Chun, K. P. Bryliakov, E. P. Talsi, V. P. Fedin and K. Kim, *Angew. Chem., Int. Ed.*, 2006, **45**, 916.

6 A. Chesney, *Green Chem.*, 1999, **1**, 209.

7 (*a*) L. Huang, H. Wang, J. Chen, Z. Wang, J. Sun, D. Zhao and Y. Yan, *Microporous Mesoporous Mater.*, 2003, **58**, 105; (*b*) C. Lin, S. Chui, S. Lo, F. Shek, M. Wu, K. Suwinska, J. Lipkowski and I. Williams, *Chem. Commun.*, 2002, 1642; (*c*) J. A. Greathouse and M. D. Allendorf, *J. Am. Chem. Soc.*, 2006, **128**, 10678.

8 (*a*) S. Kitagawa, R. Kitaura and S. Noro, *Angew. Chem., Int. Ed.*, 2004, **43**, 2334; (*b*) M. Rosseinsky, *Microporous Mesoporous Mater.*, 2004, **73**, 15; (*c*) O. Yaghi, C. Davis, G. Li and H. Li, *J. Am. Chem. Soc.*, 1997, **119**, 2861.

9 (*a*) P. D. C. Dietzel, Y. Morita, R. Blom and H. Fjellvåg, *Angew. Chem., Int. Ed.*, 2005, **44**, 6354; (*b*) M. Dincă and J. R. Long, *J. Am. Chem. Soc.*, 2005, **127**, 9376; (*c*) N. L. Rosi, J. Kim, M. Eddaoudi, B. Chen, M. O'Keeffe and O. M. Yaghi, *J. Am. Chem. Soc.*, 2005, **127**, 1504; (*d*) A. Vimont, J.-M. Goupil, J.-C. Lavalley, M. Daturi, S. Surblé, C. Serre, F. Millange, G. Férey and N. Audebrand, *J. Am. Chem. Soc.*, 2006, **128**, 3218; (*e*) H. R. Moon, N. Kobayashi and M. P. Suh, *Inorg. Chem.*, 2006, **45**, 8672; (*f*) M. Dincă, A. Dailly, Y. Liu, C. M. Brown, D. A. Neumann and J. R. Long, *J. Am. Chem. Soc.*, 2006, **128**, 16876; (*g*) P. D. C. Dietzel, B. Panella, M. Hirscher, R. Blom and H. Fjellvåg, *Chem. Commun.*, 2006, 959; (*h*) M. Dincă, W. S. Han, Y. Liu, A. Dailly, C. M. Brown and J. R. Long, *Angew. Chem., Int. Ed.*, 2007, **46**, 1419; (*i*) M. Dincă and J. R. Long, *Angew. Chem., Int. Ed.*, 2008, **47**, 6766; (*j*) S. R. Caskey, A. G. Wong-Foy and A. J. Matzger, *J. Am. Chem. Soc.*, 2008, **130**, 10870; (*k*) P. D. C. Dietzel, R. Blom and H. Fjellvåg, *Eur. J. Inorg. Chem.*, 2008, 3624; (*l*) Y. Liu, H. Kabbour, C. M. Brown, D. A. Neumann and C. C. Ahn, *Langmuir*, 2008, **24**, 4772.

10 Unsaturated metal sites within inorganic and hybrid materials have formerly been shown to improve hydrogen adsorption(*a*) P. M. Forster, J. Eckert, J.-S. Chang, S.-E. Park, G. Férey and A. K. Cheetham, *J. Am. Chem. Soc.*, 2003, **125**, 1309; (*b*) M. R. Hartman, V. K. Peterson, Y. Liu, S. S. Kaye and J. R. Long, *Chem. Mater.*, 2006, **18**, 3221; (*c*) P. M. Forster, J. Eckert, B. D. Heiken, J. B. Parise, J. W. Yoon, S. H. Jhung, J.-S. Chang and A. K. Cheetham, *J. Am. Chem. Soc.*, 2006, **128**, 16846.

11 (*a*) S. R. Caskey, A. G. Wong-Foy and A. J. Matzger, *J. Am. Chem. Soc.*, 2008, **130**, 10870; (*b*) P. D. C. Dietzel, R. E. Johnsen, H. Fjellvåg, S. Bordiga, E. Groppo, S. Chavan and R. Blom, *Chem. Commun.*, 2008, 5125; (*c*) P. D. C. Dietzel, V. Besikiotis and R. Blom, *J. Mater. Chem.*, 2009, **19**, 7362; (*d*) D. Britt, H. Furukawa, B. Wang, T. G. Glover and O. M. Yaghi, *Proc. Natl. Acad. Sci. U. S. A.*, 2009, **106**, 20637.

12 (*a*) L. Alaerts, C. Kirschhock, M. Maes, M. van der Veen, V. Finsy, A. Depla, J. Martens, G. Baron, P. Jacobs, J. Denayer and D. E. De Vos, *Angew. Chem., Int. Ed.*, 2007, **46**, 4372; (*b*) M. Maes, L. Alaerts, F. Vermoortele, R. Ameloot, S. Couck, V. Finsy, J. Denayer and D. E. De Vos, *J. Am. Chem. Soc.*, 2010, **132**, 2284.

 This journal is © The Royal Society of Chemistry 2012

View Article Online

13 M. Maes, M. Trekels, M. Boulhout, S. Schouteden, F. Vermoortele, L. Alaerts, D. Heurtaux, Y.-K. Seo, Y. K. Hwang, J.-S. Chang, I. Beurroies, R. Denoyel, K. Temst, A. Vantomme, P. Horcajada, C. Serre and D. E. De Vos, *Angew. Chem., Int. Ed.*, 2011, **50**, 4210.
14 K. Cychosz, A. Wong-Foy and A. Matzger, *J. Am. Chem. Soc.*, 2008, **130**, 6938.
15 B. Kesanli and W. Lin, *Coord. Chem. Rev.*, 2003, **246**, 305.
16 S. S. Y. Chui, S. M. F. Lo, J. P. H. Charmant, A. G. Orpen and I. D. Williams, *Science*, 1999, **283**, 1148.
17 M. Dincă, A. Dailly, Y. Liu, C. M. Brown, D. A. Neumann and J. R. Long, *J. Am. Chem. Soc.*, 2006, **128**, 16876.
18 G. Férey, C. Mellot-Draznieks, C. Serre, F. Millange, J. Dutour, S. Surblé and I. Margiolaki, *Science*, 2005, **309**, 2040.
19 S. Horike, M. Dincă, K. Tamaki and J. R. Long, *J. Am. Chem. Soc.*, 2008, **130**, 5854.
20 (*a*) A. Dhakshinamoorthy, M. Alvaro and H. Garcia, *ACS Catal.*, 2011, **1**, 48; (*b*) A. Dhakshinamoorthy, M. Alvaro and H. Garcia, *ChemCatChem*, 2010, **2**, 1438; (*c*) A. Dhakshinamoorthy, M. Alvaro and H. Garcia, *Chem. Commun.*, 2010, **46**, 6476; (*d*) J. Kim, S. Bhattacharjee, K.-E. Jeong, S.-Y. Jeong and W.-S. Ahn, *Chem. Commun.*, 2009, 3904.
21 A. Dhakshinamoorthy, M. Alvaro and H. Garcia, *J. Catal.*, 2009, **267**, 1.
22 A. Dhakshinamoorthy, M. Alvaro and H. Garcia, *Chem.–Eur. J.*, 2010, **16**, 8530.
23 A. Dhakshinamoorthy, M. Alvaro and H. Garcia, *Adv. Synth. Catal.*, 2009, **351**, 2271.
24 A. Dhakshinamoorthy, M. Alvaro and H. Garcia, *Adv. Synth. Catal.*, 2010, **352**, 3022.
25 A. Dhakshinamoorthy, M. Alvaro and H. Garcia, *Appl. Catal., A*, 2010, **378**, 19.
26 Y. K. Hwang, D.-Y. Hong, J.-S. Chang, H. Seo, M. Yoon, J. Kim, S. H. Jhung, C. Serre and G. Férey, *Appl. Catal., A*, 2009, **358**, 249.
27 Y. K. Hwang, D.-Y. Hong, J.-S. Chang, S. H. Jhung, Y.-K. Seo, J. Kim, A. Vimont, M. Daturi, C. Serre and G. Férey, *Angew. Chem., Int. Ed.*, 2008, **47**, 4144.
28 A. Dhakshinamoorthy, M. Alvaro and H. Garcia, *Adv. Synth. Catal.*, 2010, **352**, 711.
29 L. Alaerts, E. Séguin, H. Poelman, F. Thibault-Starzyk, P. A. Jacobs and D. E. De Vos, *Chem.–Eur. J.*, 2006, **12**, 7353.
30 M. Dincă, W. S. Han, Y. Liu, A. Dailly, C. M. Brown and J. R. Long, *Angew. Chem., Int. Ed.*, 2007, **46**, 1419.
31 K. Sumida, S. Horike, S. S. Kaye, Z. R. Herm, W. L. Queen, C. M. Brown, F. Grandjean, G. J. Long, A. Dailly and J. R. Long, *Chem. Sci.*, 2010, **1**, 184.
32 W. Ouellette, K. Darling, A. Prosvirin, K. Whitenack, K. R. Dunbar and J. Zubieta, *Dalton Trans.*, 2011, **40**, 12288.
33 (*a*) J. Huang, T. Akita, J. Faye, T. Fujitani, T. Takei and M. Haruta, *Angew. Chem., Int. Ed.*, 2009, **48**, 7862; (*b*) A. K. Sinha, S. Seelan, S. Tsubota and M. Haruta, *Angew. Chem., Int. Ed.*, 2004, **43**, 1546.
34 (*a*) N. Komiya, T. Naota, Y. Oda and S. I. Murahashi, *J. Mol. Catal. A: Chem.*, 1997, **117**, 21; (*b*) A. Boettcher, M. W. Grinstaff, J. A. Labinger and H. B. Gray, *J. Mol. Catal. A: Chem.*, 1996, **113**, 191.
35 W. W. Wendlandt and H. G. Hecht, *Reflectance Spectroscopy*, Interscience Publishers/JohnWiley & Sons, New York, 1966.
36 (*a*) G. M. Sheldrick, *SHELXTL Version 5.1*, Bruker Analytical X-ray Instruments Inc., Madison, Wisconsin, USA, 1998; (*b*) G. M. Sheldrick, *SHELX-97 PC Version*, University of Göttingen, Germany, 1997.
37 L. Alaerts, M. Maes, M. van der Veen, P. Jacobs and D. E. De Vos, *Phys. Chem. Chem. Phys.*, 2009, **11**, 2903.
38 M. Dincă and J. Long, *J. Am. Chem. Soc.*, 2007, **129**, 11172.
39 V. A. Blatov, *IUCr CompComm Newsletter*, 2006, **7**, 4.
40 Reticular Chemistry Structure Resource, (http://okeeffews1.la.asu.edu/RCSR/home.htm).
41 M. J. Bucknum and E. A. Castro, *Cent. Eur. J. Chem.*, 2005, **3**, 169.
42 (*a*) S. Ma and H.-C. Zhou, *J. Am. Chem. Soc.*, 2006, **128**, 11734; (*b*) S. B. Choi, M. J. Seo, M. Cho, Y. Kim, M. K. Jin, D.-Y. Jung, J.-S. Choi, W.-S. Ahn, J. L. C. Rowsell and J. Kim, *Cryst. Growth Des.*, 2007, **7**, 2290; (*c*) Y.-X. Tan, Y.-P. He and J. Zhang, *Chem. Commun.*, 2011, **47**, 10747.
43 A. L. Spek, *J. Appl. Crystallogr.*, 2003, **36**, 7.
44 T. J. Markley, B. H. Toby, R. M. Pearlstein and D. Ramprasad, *Inorg. Chem.*, 1997, **36**, 3376.
45 (*a*) J.-Y. Zhang, Y.-Q. Yang, H.-Q. Peng, A.-L. Cheng and E.-Q. Gao, *Struct. Chem.*, 2008, **19**, 535; (*b*) T. Jiang, Y.-F. Zhao and X.-M. Zhang, *Inorg. Chem. Commun.*, 2007, **10**, 1194; (*c*) W.-C. Song, J.-R. Li, P.-C. Song, Y. Tao, Q. Yu, X.-L. Tong and X.-H. Bu, *Inorg. Chem.*, 2009, **48**, 3792; (*d*) Y. Li, X. H. Zhong, F.-K. Zheng, M.-F. Wu, Z. F. Liu and G.-C. Guo, *Inorg. Chem. Commun.*, 2011, **14**, 407; (*e*) Y. Li, G. Xu, W.-Q. Zou, M.-S. Wang, F.-K. Zheng, M.-F. Wu, H.-Y. Zeng, G.-C. Guo and J.-S. Huang, *Inorg. Chem.*, 2008, **47**, 7945.
46 (*a*) A. B. P. Lever, *Inorganic Electronic Spectroscopy*, Elsevier Publishing Company, Amsterdam, 1968, ch. 9; (*b*) The *Dq* and *B* values were estimated by using the transition energy ratio diagrams in pp. 393–400 of the same book as in ref. 46*a*.
47 (*a*) X. Wang, L. Liu and A. Jacobsen, *Angew. Chem., Int. Ed.*, 2006, **45**, 1; (*b*) P. Horcajada, C. Serre, M. Vallet-Regi, M. Sebban, F. Taulelle and G. Férey, *Angew. Chem., Int. Ed.*, 2006, **45**, 5974.
48 Y. Ishii, S. Sakaguchi and T. Iwahama, *Adv. Synth. Catal.*, 2001, **343**, 393.
49 A. Dhakshinamoorthy, M. Alvaro and H. Garcia, *Chem.–Eur. J.*, 2011, **17**, 6256.

Published on 03 February 2012 on http://pubs.rsc.org | doi:10.1039/C2JM15592C
Downloaded by Instituto de Tecnología Química on 18/04/2013 15:49:46.